Title

Screening Aluminum-Based Compounds as Low-k Dielectrics for High-Frequency Applications

Journal

Chemistry of Materials, 36(3)

ISSN

0897-4756 1520-5002

Authors

Morgan, Emily E

Zohar, Arava

Lipkin, Sophia

et al.

Publication Date

2024-02-02

DOI

10.1021/acs.chemmater.3c01975

Peer reviewed

Screening Aluminum-Based Compounds as Low-κ Dielectrics for High-Frequency Applications

Emily E. Morgan,[†,‡] Arava Zohar,[†,‡] Sophia Lipkin,[¶] Bartomeu Monserrat,[§] Subramanian Vaidyanathan,[‖] Daniel Loeffler,[‖] Rui Zhang,[⊥] Kerstin Schierle-Arndt,[‖] Anthony K. Cheetham,[‡,#] and Ram Seshadri[*,‡,¶]

†*These authors contributed equally to this work*

‡*Materials Department and Materials Research Laboratory*

University of California, Santa Barbara, California 93106, United States

¶*Department of Chemistry and Biochemistry*

University of California, Santa Barbara, California 93106, United States

§*Department of Materials Science and Metallurgy and Cavendish Laboratory*

University of Cambridge, Cambridge CB3 0FS, United Kingdom

‖*BASF SE, 67056 Ludwigshafen am Rhein, Germany*

⊥*California Research Alliance (CARA)*

BASF Corporation, Berkeley, California 94720, United States

#*Department of Materials Science and Engineering*

National University of Singapore, Singapore 117575, Singapore

E-mail: seshadri@mrl.ucsb.edu

Abstract

Advances in telecommunications require electronics that operate at ever-increasing frequencies, exemplified by 5G or fifth generation technologies that operate in the GHz regime. At high frequencies, electrical circuits are plagued by so-called RC delays, arising from the time constant $\tau = RC$ for electrical signals which is the product of the resistance R and the capacitance C, respectively, of conductors and their insulating substrates. Beside using high quality, low-R electrical conductors such as high-purity Cu with low surface roughness, small RC delays are achieved by lowering the dielectric constant κ of the materials used in printed circuit board (PCB) substrates. These largely comprise particles of an inorganic material, notably functionalized SiO_2, embedded in a polymer-based matrix. The value of κ of the composite is primarily dictated by κ of the inorganic material. The properties of the inorganic component also impact other relevant parameters such the quality factor, mechanical strength, and thermal expansion of the substrate. Here we ask whether there are inorganic compounds with dielectric constants (measured at 10 GHz) that are lower than that of SiO_2 that could potentially replace it in electronics. We describe the key characteristics for low-κ materials and develop a framework for screening such compounds by employing some guiding principles, followed by using a combination of empirical estimates and density functional perturbation-theory based calculations. We then report experimental results on two promising, aluminum-based low-κ compounds for high-frequency applications. The first is the cristobalite form of $AlPO_4$. The second is the simplest 3D metal-organic framework, aluminum formate $Al(HCOO)_3$. The measured values of κ at 10 GHz, which are 4.0 for $AlPO_4$ and 3.8 for $Al(HCOO)_3$, compare well with what is measured on SiO_2 particles.

Introduction

The implementation of fifth-generation (5G) telecommunications technology promises many significant advancements in data networks, including faster, more reliable, and cheaper communication. One barrier to realizing these potential benefits is that current hardware must be optimized for compatibility with the high-frequency ranges used in 5G networks. An example of this can be found in the development of specialized electronics used for multiple-input multiple-output antennae in 5G handsets and base stations. The ideal dielectric material for use in these electronics should possess a low dielectric constant (κ) and low loss at the frequencies of interest, and should allow for effective thermal and thermomechanical management. Critically, the material with the lowest dielectric constant will produce the most efficient antenna, which in turn will reduce power consumption in devices.[1]

Identification of materials that have all of these necessary characteristics is a challenge for widespread implementation of the 5G technology. Furthermore, the need for low-κ and low-loss materials extends beyond 5G applications to other types of advanced electronics that rely on printed circuit board (PCB) technology.[2,3] In general, the operational speed of a circuit is limited by its time constant $\tau = RC$, the product of the resistance R and capacitance C. As circuits become smaller, with thinner wires placed closer together, the resistance of the wires and capacitive effects between them increase, causing longer delays. Given that circuit miniaturization is required to produce advanced devices, a critical strategy to lower τ is to reduce capacitive effects by using a PCB material with a low dielectric constant.[4]

In addition to low dielectric constant, there are several other important characteristics for the low-κ material to be used in PCBs. These include low dielectric loss, thermal and chemical stability, hydrophobicity, mechanical strength, low thermal expansion, and acceptable thermal conductivity.[3] In order to meet these requirements, a common solution is to combine a low-κ inorganic component, such as silica particles or fibers, with an organic

polymer to produce a composite which takes advantage of the best qualities of both materials. The dielectric properties of these composites can also be enhanced through a number of strategies. For example, more C–C and C–F bonds can be incorporated into the polymer to minimize polarizability and hence κ.[5] Additionally, porosity can be engineered into the composite in order to lower its density and therefore reduce the number of dipoles.[5–7]

There are several ways to reduce the dielectric constant of composites, but each often involves trade-offs with other desirable qualities. For example, the use of a larger volume fraction of the organic component relative to the inorganic component may lead to a lower dielectric constant for the composite but could produce deleterious thermal expansion effects and poor mechanical properties. Therefore, in order to further reduce the dielectric constant of PCB composites, it is important to identify materials which have the desirable qualities of silica (low loss, mechanical strength, stability, and good thermal management) while also possessing low dielectric constants (defined in this work i as being < 4.0 when measured at 10 GHz.)

While silica works well and is inexpensive, there is nevertheless an interest in finding other materials, since established limits to low-dielectric performance have not been outlined in the literature. Several materials have been proposed as alternatives to silica, including $AlPO_4$–BPO_4–SiO_2 ternaries,[4] cordierite,[8–10] and several borates.[11–13] The characteristics of these compounds suggest that compounds with low-atomic number atoms and open frameworks should be prioritized. Furthermore, the search for low-κ materials should be contrasted with efforts to find inorganic high-dielectric constant materials and ferroic materials[14–19] where traditionally second-order Jahn-Teller[20] ions such as Ti^{4+} and lone-pair ions such as Bi^{3+} are used.[21] These works actually aid in the search for low-κ materials by suggesting which ions are best avoided.

In the present work, we have focused on developing a methodology for the identification of materials with dielectric constants comparable to or lower than that of silica. The main challenges are the large number of parameters that require optimization for a suc-

cessful low-κ material and the lack of standardization in literature in reporting of dielectric constants. We have found that estimates using the additive formula[22] with empirical values tabulated by Shannon,[23] are suitable for identifying potential low-κ candidates from a large database of materials. First-principles calculations based on density functional theory (DFT) then refine the search, and also permit estimates to be made for compounds that are not appropriately parametrized for the additive formula approach. As a result of this screening procedure, we have identified the simple aluminum-based framework structures, $AlPO_4$ and the metal-organic framework $Al(HCOO)_3$ (ALF), as suitable for low-κ applications. ALF is arguably the simplest example of a metal-organic framework and has both porosity and excellent mechanical properties. It has recently been shown to be effective in a number of important gas separations.[24–26] ALF is also interesting to study in the context of some metal formate compounds being to display ferroelectric switching associated with hydrogen bonding.[27,28] It is important in this context to recognize that polar ground states are associated with aligned static dipoles, but the dielectric constant is a measure of the dynamic response of which of a the material to an external electric field. It is possible for materials to possess permanent dipoles and yet retain relatively low dielectric constants.

We have prepared these compounds and have developed and discussed different strategies for the measurement of their high-frequency dielectric properties, in powder form. Finally, we compare the case of $AlPO_4$, where DFT gives an accurate estimate of the dielectric constant, to the case of $Al(HCOO)_3$, where a simple DFT calculation does not initially correctly predict the dielectric constant. For completion, we also present DFT calculations on crystalline polyethylene (as a compound that can be compared to measurements on paraffin), and on a model for crystalline polytetrafluoroethylene, that is again compared with experiments on pressed pellets.

Methods

First-Principles Calculations

Static dielectric constants were estimated using density functional theory (DFT)-based electronic structure calculations as implemented in the Vienna ab initio Simulation Package (VASP).[29–31] All calculations used the PBE functional,[32] PAW pseudopotentials,[33,34] a plane-wave cutoff energy of 500 eV, and a Monkhorst-Pack grid[35] with a length parameter of 30. For the density functional perturbation theory calculations of the dielectric constant,[36,37] we report the predicted constant for a polycrystalline sample using Equation 1,

$$\kappa = \frac{3\lambda_1\lambda_2\lambda_3}{\lambda_1\lambda_2 + \lambda_1\lambda_3 + \lambda_2\lambda_3} \tag{1}$$

where λ_i are the eigenvalues of the total dielectric tensor calculated in VASP. This is the convention used in other high-throughput DFT studies of dielectric constants.[38] As discussed previously,[39] estimating the dielectric constant of a polycrystalline sample from the tensor components is not trivial except in the case of high symmetry crystal structures, and the formula used here will not always give the same results as other common approaches, such as averaging the eigenvalues.

Synthesis of $Al(HCOO)_3$

A hydrothermal synthesis of $Al(HCOO)_3$ was performed following the literature.[40] 50 mg (0.64 mmol) of $Al(OH)_3$ was combined with 7 mL of concentrated formic acid and stirred for 30 min. The mixture was then transferred to a polytetrafluoroethylene-lined 23 mL stainless steel digestion vessel and heated at 130 °C for 3 days. Cooling to room temperature yields a white powder, which was isolated by filtration and rinsed with concentrated ethanol. In order to remove the template CO_2 molecule from the cavities of the structure, the powder was heated at 180 °C for 24 hours.[24]

Modification of $AlPO_4$

$AlPO_4$ was purchased from Fisher Scientific; however, the as-received powder was multiphasic. In order to isolate the desired orthorhombic phase, which has the cristobalite structure, the powder was heated to 1300 °C in a furnace and allowed to equilibrate for 1 h. The sample was then removed from the furnace and allowed to cool rapidly in air.

Powder X-ray Diffraction and Rietveld Refinements

Powder X-ray diffraction (PXRD) measurements were performed on a Panalytical Empyrean powder diffractometer in reflection mode with a Cu-Kα radiation source. Rietveld analysis was performed to confirm structure and phase-purity using the TOPAS software package.[41] Crystal structures were visualized using the VESTA software package.[42]

Scanning electron microscopy

The $Al(HCOO)_3$ and $AlPO_4$ powders were placed on double sided carbon tape and inserted into an Apreo C FEG (ThermoFisher) microscope chamber. SEM images were collected using secondary electron (SE) and InLens detectors with 5 keV accelerating voltage and 0.8 nA current.

Infrared Spectroscopy

Fourier transform infrared (FTIR) spectra of powders were obtained using a Nicolet iS10 FTIR equipped with a Smart Diamond ATR accessory in absorption mode.

Pellet Preparation

Two methods of preparing pellet samples for dielectric measurements were employed. The first was a modified version of a literature procedure[43] in which different volume loadings

of inorganic particles were introduced into a paraffin wax matrix. We prepared mixtures of different ratios of melted paraffin wax and the inorganic phase of interest and drop-cast pellets of the mixtures onto polyethylene terephthalate (PET) sheets. The pellets were flattened into thin films (thickness less than 1 mm) suitable for measurement as the mixture cooled by pressing the PET sheets together.

While this first method has been shown to be reliable for measuring the dielectric constant of a variety of materials,[43] it was difficult to obtain pellets of perfectly uniform thickness. Given that the dielectric measurements are very sensitive to even small differences in thickness, it was desirable to test a second set of samples where we could control the thickness more carefully. For this set of samples, the material under investigation was ground together with polytetrafluoroethylene (PTFE) beads in an agate mortar and pestle. After grinding the materials, the mixture was placed into a pellet die with a diameter of 25.4 mm and pressed with forces up to 5 tons. Using helium pycnometry, it was estimated that this process achieves a pellet densification of between 85% and 90%.

Dielectric Property Measurements

A split-post dielectric resonator (SPDR, purchased from Keysight Technologies) was used in conjunction with a Agilent PNA model N5242A vector network analyzer (VNA) for measurements of high-frequency dielectric properties. A complete description of the method can be found in the literature.[44] In summary, two coupling loops induce a continuous electric field in the microwave frequency regime within the plane of the sample. The resonant frequency and quality factor of the SPDR will shift in the presence of a sample, and therefore the sample properties can be determined by measuring the SPDR in the absence and presence of the sample. The resonant frequency can be found with uncertainties on the order of 0.5% to 1% of the measured resonant curve bandwidth. The SPDR has a resonance frequency of 10.159 GHz and can measure samples up to 0.95 mm thick, where the sample diameter was always equal to or greater than 22 mm. The accuracy of the device

was confirmed by measurement of a fused silica reference sample included with the SPDR, which has a measured dielectric constant of 3.824.

The SPDR was calibrated by first performing transmission measurements between the two ports of the VNA in a shorted configuration using flexible SMA cables (to account for losses coming from those cables). The signal was normalized around the resonance frequency 10.159±0.500 GHz using the calibration setting of the VNA software. Following calibration, the SPDR was connected with the two SMA cables. A reflectance measurement was used to find the resonant frequency. For an empty resonator, the frequency should be similar to the device specification (10.159 GHz). A transmission measurement was recorded at the resonance frequency and the Q value was extracted from the bandwidth at 3 dB beneath the peak of the transmission curve. Next, the sample was inserted to the SPDR and the resonance frequency and Q value were recorded.

The sample thickness was determined by micrometer or SEM cross section. The collected values (resonance frequency, Q, and thickness) were entered into the software to extract the dielectric constant and the energy loss factor following Equation 2.

$$\kappa = 1 + \frac{f_0 - f_s}{h f_0 K_\kappa(\kappa_r, h)} \tag{2}$$

where h is the thickness of the sample under test, f_0 is the resonant frequency of the empty SPDR, f_s is the resonant frequency of the SPDR with the sample and K_κ is a function of κ and h determined and are obtained in the iterative procedure.[45]

In order to determine the dielectric constant of solid inorganic materials, pellets were prepared as described in the previous section and their dielectric constants were measured. The data for pellets of various compositions was then fit the the Looyenga mixing model,[46] which is shown in Equation 3.

$$\kappa_{mix}^{1/3} = V_m \kappa_m^{1/3} + V_p \kappa_p^{1/3} \tag{3}$$

where κ_m and κ_p are the dielectric constants of the organic matrix and inorganic particles, respectively, and V_m and V_p are their volume fractions.

Results and Discussion

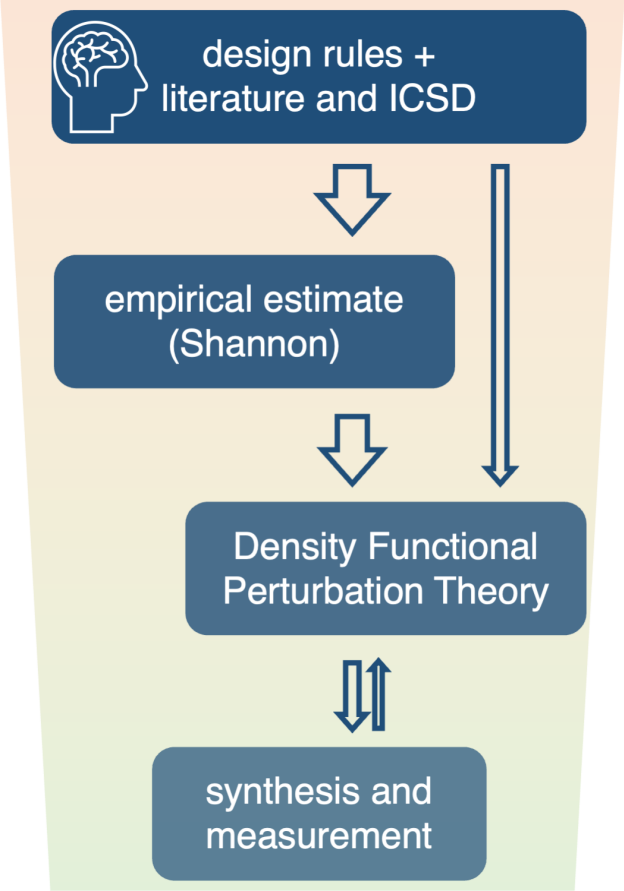

Figure 1: Workflow for the identification of low-κ materials.

There are several strategies for estimating the dielectric constant of materials, including empirical estimates,[23,47] machine-learning,[48] and high-throughput DFT.[38] In our work, we have focused on using a combination of physics-based principles to select a set of compounds on which we have carried out empirical estimates and DFT calculations. The strategy is outlined in Figure 1. The first step was to establish a set of criteria for low-κ compounds, based on the literature.[22,49] These principles are used to screen the Inorganic

Crystal Structure Database (ICSD)[50] to identify candidate materials. The criteria are that materials must be (i) insulating, (ii) stable under ambient conditions and (relatively) easy to synthesize, (iii) primarily comprise small (low-atomic-number) and high-charge atoms, (iv) crystallize in structures with extended connectivity — molecular structures and salts are usually undesirable, and (v) display low-density, which means that structures with corner-shared coordination polyhedra are prioritized over those with edge- or face-shared polyhedra. Finally, disperse bands are contraindicated for low dielectric constants at high frequencies, suggesting that highly covalent 3D networks (diamond for example) would not be suitable targets. Diamond has light atoms and a relatively open, yet highly rigid structure, suggesting that it might have a low dielectric constant.However, the nature of its semiconducting electronic structure results in it famously possessing high refractive index which is contraindicated for low κ; dielectric constants usually vary as the square of the refractive index,[49] and indeed, diamond is reported to have $\kappa = 5.87$ at MHz frequencies.[51]

A class of compounds that meets many of the above criteria are aluminosilicate zeolites, due to their porous nature and low-atomic-number components.[52] However, many zeolites are hydrophilic or are otherwise prone to incorporating small molecules in their cages, making many of them unsuitable as stable low-κ dielectrics. The Materials Project[38,53] is a useful resource for the screening of low-κ materials using, with some care being required for newer materials. Of the experimentally-observed materials reported in the Materials Project with low dielectric constants, several are molecular structures that may not be useful as SiO_2 replacements. Yet other materials have small band gaps or unpaired electrons, and their calculated dielectric constants must be considered with care.

The second step, after identifying a number of inorganic compounds is to empirically predict the dielectric constants. The estimate used here is based upon the Clausius-Mosotti equation for the dielectric constant, where each ion is assigned an empirically-determined value for its dielectric polarizability α_i, for ion i estimated and tabulated by Shannon for oxides and fluorides[23] that is partly reproduced in Table 1. The equation, presented in

Table 1: Values of the ionic polarizability α in units of $Å^{-3}$ for select ions as suggested by Shannon.[23]

Li^+	Be^{2+}	B^{3+}		O^{2-}	F^-
1.20	0.19	0.05		2.01	1.62
Na^+	Mg^{2+}	Al^{3+}	Si^{4+}	P^{5+}	
1.80	1.32	0.79	0.87	1.22	
K^+	Ca^{2+}	Ga^{3+}	Ge^{4+}		
3.83	1.50	1.63	1.72		

Equation 4, only requires the contents of the unit cell (number and type of each ion) and its volume as inputs.

$$\kappa_{\text{emp.}} = \frac{\tilde{V} + 2\alpha(4\pi/3)}{\tilde{V} - \alpha(4\pi/3)} \tag{4}$$

Here, $\alpha = \Sigma_i \nu_i \alpha_i$ with ν_i being the stoichiometry coefficient of component i, and $\tilde{V}$ is the molar volume from the associated ICSD crystallographic information files (CIF) file. A Python script was written to parse CIF files and calculate the expected dielectric constants. This script is available in the Supporting Information. A drawback of this method is that the parametrization has been limited to oxide and fluoride crystal structures, an so it is not suitable for all materials. Additionally, this equation is not accurate for compounds with unusual dielectric properties, such as ferroelectrics or conductive materials, and it does not account for the frequency-dependence of the dielectric constant.[23] Given that we had already selected compounds with low atomic number element compositions, the estimated $\kappa_{\text{emp.}}$ were all fairly low ($<$10). However, this step was still important to confirm our selection criteria and provide a preliminary ranking for which materials should be further investigated.

After calculating $\kappa_{\text{emp.}}$, DFT calculations were performed to provide a potentially more accurate estimate of the dielectric constant κ_{DFT}. This step was particularly important in order to validate the results of the empirical estimation and to estimate the dielectric constant for compounds where the additive formula could not be applied because of an

absence of the requisite parametrization. Here, we have focused on calculating the static dielectric constant, which is the sum of the electronic and ionic contributions to polarization. A full frequency dependence was not calculated because of the greater computational expense and because the static constant was expected to be similar to what would be predicted for the GHz regime in a frequency-dependent calculation. We additionally note that these DFT calculations were performed on CIF files obtained from the ICSD and literature without performing geometry optimization.

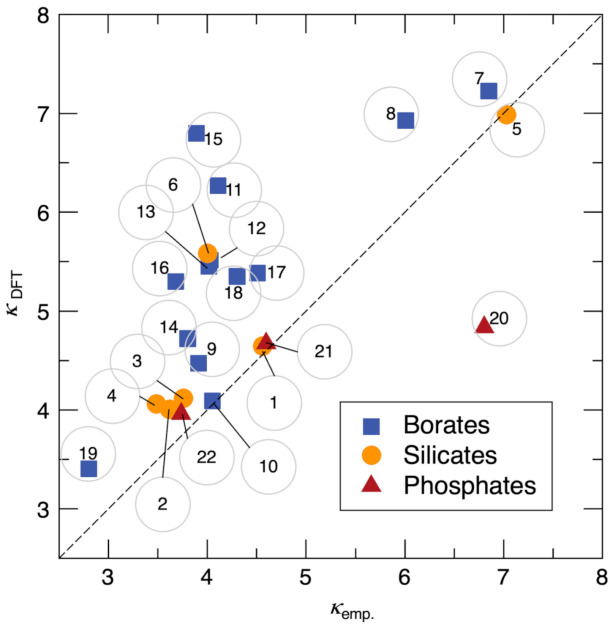

Figure 2: Plot of the DFT-calculated dielectric constant versus the associated empirical estimates using the Shannon parametrization. The samples identities corresponding to the numbering numbers are listed in Table 2.

The results of some of the DFT-calculated dielectric constants plotted against their associated empirical values are shown in Figure 2. The calculated values are also shown in Table 2. The compounds represented in this plot are those identified by our screening criteria or those reported in the literature as potential low-κ materials, such as SiO_2. In nearly all cases, the dielectric constant estimated by DFT is larger than that estimated by the Shannon parametrization. This is consistent with other work on DFT calculations, which has found that DFT tends to overestimate the dielectric constant.[38]

Table 2: Estimated dielectric constants for crystalline compounds of interest using the empirical formula ($\kappa_{\text{emp.}}$) based on the Shannon parametrization (when possible) and density functional perturbation theory calculations (κ_{DFT}). The numbers refer to the labeling in Figure 2. ICSD codes are provided when available. [a]Cambridge Crystallographic Data Center.[54] Ref. (i) is reference[55] and Ref. (ii) is reference.[24]

Material	$\kappa_{\text{emp.}}$	κ_{DFT}	ICSD code	Material	$\kappa_{\text{emp.}}$	κ_{DFT}	ICSD code
1. SiO_2 (quartz)	4.56	4.65	16331	13. $Na_2B_6O_{10}$	4.02	5.45	2045
2. SiO_2 (tridymite)	3.62	4.01	1109	14. NaB_4O_6F	3.80	4.72	112376
3. SiO_2 (α-cristobalite)	3.76	4.12	75300	15. $Na_3Al_2B_7O_{15}$	3.89	6.80	2119823[a]
4. SiO_2 (β-cristobalite)	3.48	4.06	77458	16. $Na_3AlB_8O_{15}$	3.68	5.30	2119822[a]
5. Mg_2SiO_4	7.03	6.99	12124	17. $Na_3B_7O_{12}$	4.51	5.38	99049
6. $Mg_2Al_4Si_5O_{18}$	4.00	5.59	156362	18. $Na_2B_8O_{13}$	4.30	5.35	95868
MgF_2	5.25	5.13	394	19. H_3BO_3	2.80	3.40	255723
$NaSbF_6$	N.A.	4.45	77919	20. BPO_4	6.80	4.84	55082
7. $Mg_3B_2O_6$	6.85	7.23	31385	21. $AlPO_4$ (hex.)	4.60	4.67	9641
8. $Mg_2B_2O_5$	6.01	6.93	79721	22. $AlPO_4$ (ortho.)	3.74	3.96	16651
9. $Li_2B_3O_4F_3$	3.91	4.47	423661	α-$Al(H_2PO_2)_3$	N.A.	3.96	14725
10. LiB_6O_9F	4.05	4.09	420286	γ-$Al(H_2PO_2)_3$	N.A.	4.05	1888648[a]
11. $Na_2B_4O_7$	4.11	6.27	2040	$Al(HCOO)_3$	N.A.	3.14	Ref. (ii)
12. $Na_2B_6O_9F_2$	4.03	5.51	Ref. (i)	$Al(OH)(COOH)_2$	N.A.	3.91	131852

A notable exception to this trend is BPO_4, whose empirical constant is 6.8, while the estimated constant from DFT is 4.8. Furthermore, other boron-based materials on this plot also show significant differences between the empirical value and the DFT prediction. The additive formula predicts several of them to have $\kappa < 4.5$, but their predicted constants based on DFT are significantly higher. The poor correspondence between DFT-calculated and empirically predicted values of the dielectric constant for boron-containing compounds could arise because of inadequate parametrization perhaps related to difficulties in experimentally obtaining accurate x-ray crystal structures of compounds with very light atoms like boron. Overall, we find that in most cases, the DFT-calculated value can be considered an upper limit for the estimate of the dielectric constant, while value estimated from the Shannon parametrization can be considered a lower limit.

Considering the results of the DFT calculations, we found that only a few materials had predicted dielectric constants that were comparable to that of SiO_2. These were $AlPO_4$ (κ_{DFT} = 3.96), $Al(H_2PO_2)_3$ (κ_{DFT} = 3.96), and $Al(HCOO)_3$ (κ_{DFT} = 3.14). In the case of

$AlPO_4$, the constant estimated from the additive formula was slightly lower, at 3.73. For the other materials, which are hybrid organic-inorganic structures, it was not possible to calculate the empirical value, as no polarizability values are available for the organic components. To validate our predictions, we chose to focus on the dielectric constants of $AlPO_4$ and $Al(HCOO)_3$. These compounds were selected because $AlPO_4$ has been previously reported as a potential low-κ material, while $Al(HCOO)_3$ has the lowest DFT-estimated constant of any material that we investigated and has not been previously considered as a low-κ material.

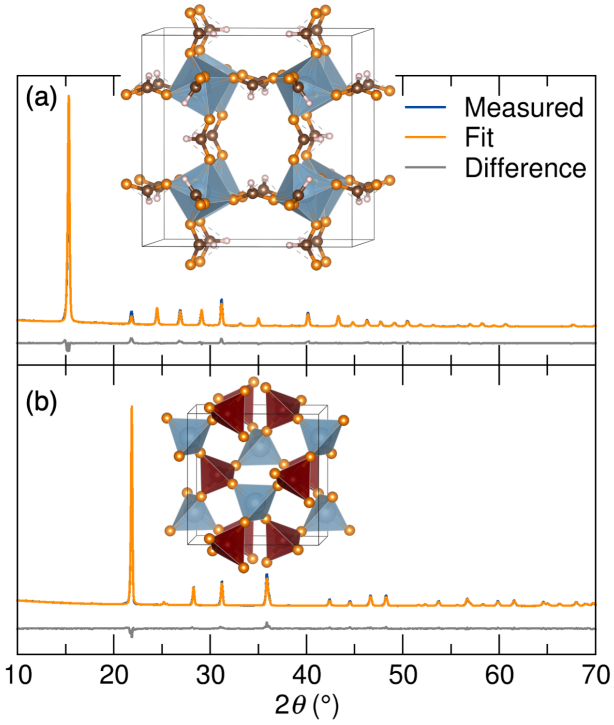

Figure 3: Powder X-ray diffraction patterns and Rietveld refinements for (a) $Al(HCOO)_3$ and (b) $AlPO_4$. Insets show the crystal structures of the two compounds.

In order to investigate the dielectric properties of $AlPO_4$ and $Al(HCOO)_3$, it was important to obtain phase-pure samples of these materials. $Al(HCOO)_3$ can be synthesized on the gram scale using hydrothermal synthesis, as reported in the literature.[40] During the synthesis, CO_2 molecules template the formation of the structure and should be removed from the cavities by heating the material to 180 °C for 24 hours.[24] The removal of CO_2

was confirmed using FTIR spectroscopy, shown in the Supporting Information. The PXRD pattern and Rietveld refinement for $Al(HCOO)_3$ confirming phase-purity after heating are shown in Figure 3(a). In the case of $AlPO_4$, the material is purchased from commercial vendors. However, we have observed that the powder is often received as a mix of polymorphs. In order to obtain the pure orthorhombic phase, which was estimated to have the lowest dielectric constant, the powder required heat-treatment. The powder was heated to 1300 °C, held at that temperature for one hour, and then the crucible was removed from the furnace to cool in air. The PXRD patterns and Rietveld refinements shown in Figure 3(b) confirm that the material is single-phase following this procedure.

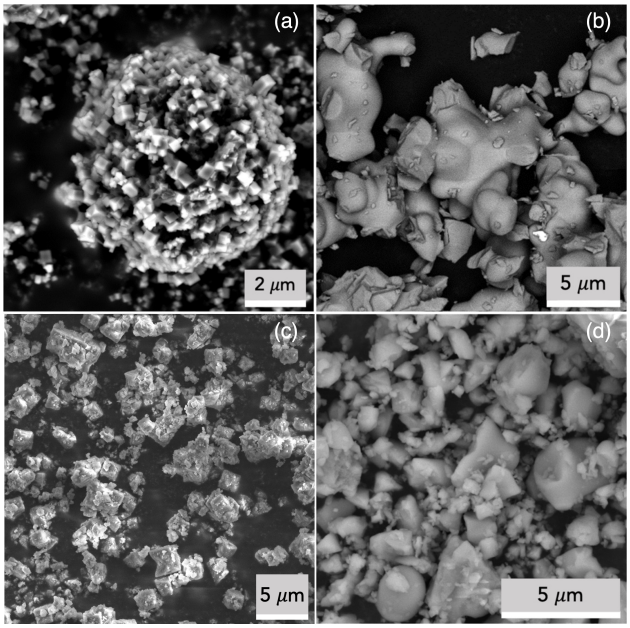

Figure 4: SEM images of (a) $Al(HCOO)_3$ and (b) $AlPO_4$ before and (c) $Al(HCOO)_3$ and (d) $AlPO_4$ after ball-milling.

After confirming phase purity using XRD, SEM was used to demonstrate that the samples were homogeneous and that no amorphous phases were present. SEM images of $Al(COOH)_3$ and $AlPO_4$ particles are shown in Figure 4. In the case of $Al(HCOO)_3$, the as-synthesized particles are cube-shaped with a typical edge length ranging from 100 nm to 500 nm. These small cubes tend to form spherical aggregates which are 5 μm to 10 μm in diameter. For the $AlPO_4$, we observed globule-shaped particles whose size was also on

the order of 10 μm. These larger aggregates and particles are not necessarily a problem for the measurement of dielectric properties. However, in practical applications, the particle size would need to be reduced to $< 1\mu$m in order to produce homogeneous films. We therefore ball-milled samples to reduce particle size. In $Al(HCOO)_3$, the small cube-shaped particles remain after 30 minutes of ball-milling, but the larger spherical aggregates are not observed. For $AlPO_4$, SEM images show that ball-milling effectively breaks the larger particles into smaller fragments. In both cases, XRD confirms that the underlying crystal structure remains intact. This observation is in agreement with previous reports which demonstrate that, unlike other metal-organic frameworks, $Al(HCOO)_3$ is mechanically robust.[24] In summary, with proper post-synthetic modification, both materials could potentially be incorporated into epoxy substrates for PCB applications.

As a next step, we measured dielectric constants at high frequencies (close to 10 GHz). A split post dielectric resonator (SPDR) device connected to a vector network analyzer (VNA) was employed, as described in the Methods section. This allowed us to reliably measure many samples because it does not require contact deposition or customized hardware. The SPDR is primarily designed for measuring composite films similar to PCB materials. The method requires powders to be embedded in an organic matrix to form a thin film with a diameter larger than 22 mm. For each inorganic material, the dielectric constant can be evaluated by making samples with different ratios of inorganic particles to organic matrix material. The dielectric constants of these samples are subsequently measured, and the results fit to the Looyenga mixing model.[46] This model takes into account the dielectric constants of the pure components and their volumetric fraction in the mixture.

As discussed in the Methods section, two types of samples were prepared in order to measure the dielectric constants of inorganic powders. Each of these methods has its own benefits and drawbacks. In the case of the paraffin pellets, the main advantage is that it is easier to control the precise composition of the mixture, which makes the data most suitable for modeling with the Looyenga mixing model. However, the drawback to this

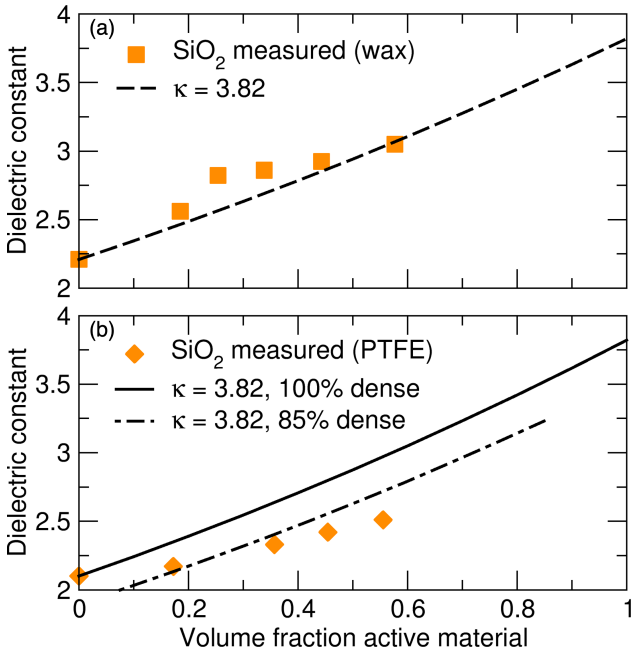

Figure 5: (a) Measured dielectric constants for SiO_2 and paraffin wax pellets and fit to Looyenga model with $\kappa = 3.82$. (b) Measured dielectric constants for SiO_2 and PTFE pellets and fits to Looyenga model with $\kappa = 3.82$ accounting for different levels of densification. The measurement frequency was 10.159 GHz.

method is that the drop-cast mixture must be flattened into a thin film as the mixture cools, which often leads to inhomogeneity in the thickness of the films. Additionally, it is difficult to produce films that have larger volume fractions of the inorganic material, as the solidified mixtures become very brittle. For these reasons, we also produced a second set of samples which were mixtures of PTFE and the inorganic particles. These samples were prepared by grinding the materials in a mortar and pestle and pressing them together using a pellet die and hydraulic press. This method is effective because grinding the PTFE beads forms sheets which can encapsulate the inorganic powder, and the samples can be pressed to a very uniform thickness. However, the disadvantage of this method is that it was not possible to achieve 100% densification of the pellets. Therefore, in order to interpret the dielectric data, the role of air must be accounted for in the mixing model, which adds additional uncertainty to the interpretation of the data for these samples. In order to evaluate the effectiveness of both sample-preparation methods, we used fumed

silica powder as a test material, which is known to have a dielectric constant of 3.82. The results for both sets of measurements are shown in Figure 5.

First considering the results for the silica and paraffin wax pellets, we find that the data fits fairly well to the Looyenga mixing model when the dielectric constant of the pure wax is assumed to be 2.2 and the constant of pure silica is 3.82. However, for some of the intermediate compositions there is a discrepancy between the measured data and the model, which is likely due to variation in the thicknesses of some of the samples. Next, considering the PTFE data, we find that the measured dielectric constants for the pellets are much lower than would be expected if the pellets were 100% dense. Here, the dielectric constant of PTFE is assumed to be 2.1,[56] and silica again is 3.82. Therefore, in this case we needed to add air as an additional "component" in the Looyenga model and adjust the volume fractions of the silica and PTFE accordingly. Using this method, we find that the best match to our data corresponds to a densification of approximately 85%. This is in good agreement with pycnometry measurements of the pellets, which indicated a densification of approximately 90%. We find that the fit is not as good for larger volume fractions of silica, which can be attributed to the fact that the densification may be dependent on the composition of the pellet. Overall, we find that the paraffin wax method provides a more reliable measurement of the dielectric constant, but that PTFE pellets can be used to corroborate the results.

Given the results of the dielectric measurements for the silica pellets, we have used paraffin wax pellets to estimate the dielectric constants of our two candidate materials. The measurements and data fitting for paraffin pellets of $Al(HCOO)_3$ and $AlPO_4$ are shown in Figure 6. Again using the Looyenga mixing model, the dielectric constants were determined to be 3.8 for $Al(HCOO)_3$ and 4.0 for $AlPO_4$. Just as in the case of the silica pellets, we have also confirmed these values by measuring mixtures of our candidate materials with PTFE. These measurements and fits to the data are shown in the Supporting Information. In the case of $AlPO_4$, the measured value is very close to the value of 3.96 predicted

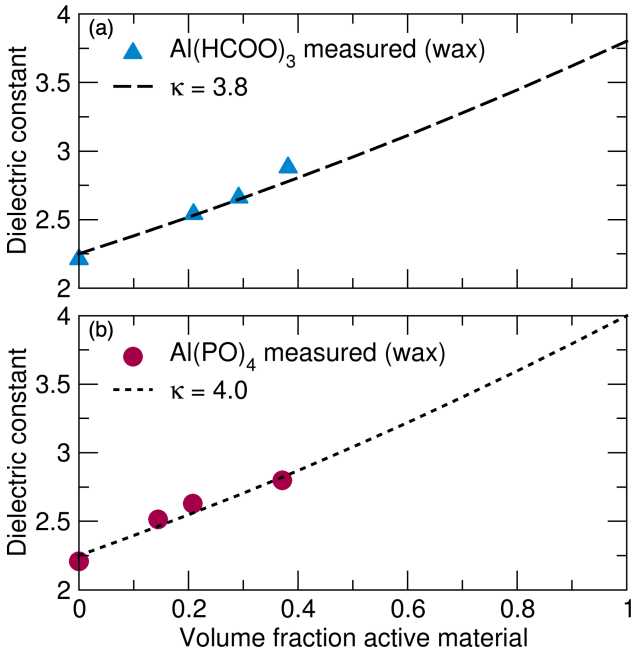

Figure 6: Measured dielectric constants for (a) $Al(HCOO)_3$ and paraffin wax pellets (b) $AlPO_4$ and paraffin wax pellets. The measurement frequency was 10.159 GHz.

by DFT. However, for $Al(HCOO)_3$, there is a significant difference between the measured value of 3.8 and the value of 3.14 predicted by DFT. This finding is also somewhat unusual in that it represents a case in which the experimental dielectric constant is higher than the DFT prediction.

We hypothesized that the discrepancy between theory and experiment for $Al(HCOO)_3$ may be due to finite temperature effects which were not accounted for in the DFT calculation, or inaccuracies in the position of the organic linkers in our structural model. Therefore, we have further investigated how changes to the $Al(HCOO)_3$ structure may influence the calculated dielectric constant. In Figure 7, we show the crystal structure of $Al(HCOO)_3$ determined from Rietveld refinements of neutron diffraction data superimposed with the structure that results from relaxing the atomic positions in DFT using the PBE functional. The first crystal structure was used in our original DFT calculations and gives the predicted dielectric constant of 3.14. We also calculated the constant for the relaxed structure and obtained a value of 4.14. The main difference between the two calculated values lies in a change in the ionic contribution to the dielectric constant, where the original structure has

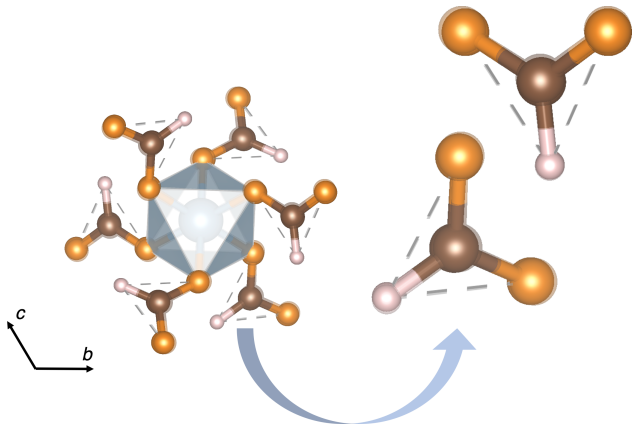

Figure 7: Crystal structure fragment of $Al(HCOO)_3$ at 300 K determined from neutron diffraction superimposed with the structure obtained by relaxing the atomic positions in DFT.

an ionic component of 1.15, while in the relaxed structure the value is 2.12. This result is somewhat surprising, as the changes to the crystal structure are extremely small, indicating that the ionic component of the calculated dielectric constant is strongly dependent on the atomic positions in this structure.

In order to determine whether the sensitivity of κ_{DFT} to structure is common to different types of compounds, we also investigated the effects of DFT relaxation on other compositions studied in this work. For example, in $AlPO_4$, we found that the value of κ_{DFT} changed from 3.96 (experimental structure) to 3.98 (atomic positions relaxed with PBE-DFT). The more significant change for $Al(HCOO)_3$ was consistent with our idea that the presence of the organic linker may contribute significantly to the dielectric constant for this compound. For this reason, we also used DFT to predict the dielectric constants of polyethylene and PTFE. For PTFE, there is no crystal structure available for ambient conditions, so a structure was generated by changing the polyethylene structure such that all H atoms were replaced with F, and the atomic positions and cell parameters were allowed to relax to their lowest energy positions in DFT. The relaxed structures are shown in Figure 8 and we confirmed that the bond distances and angles for the relaxed polyethylene and PTFE were realistic by comparison with literature reports.[59–61]

In the case of polyethylene, the calculated value of κ_{DFT} is 2.52 based on the experi-

(a) polyethylene, *Pnma*

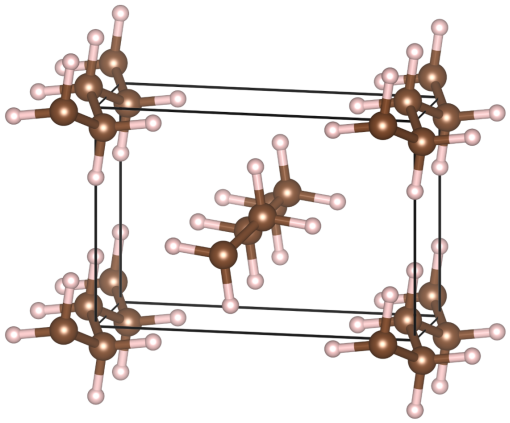

(b) polytetrafluoroethylene, *Pnma*

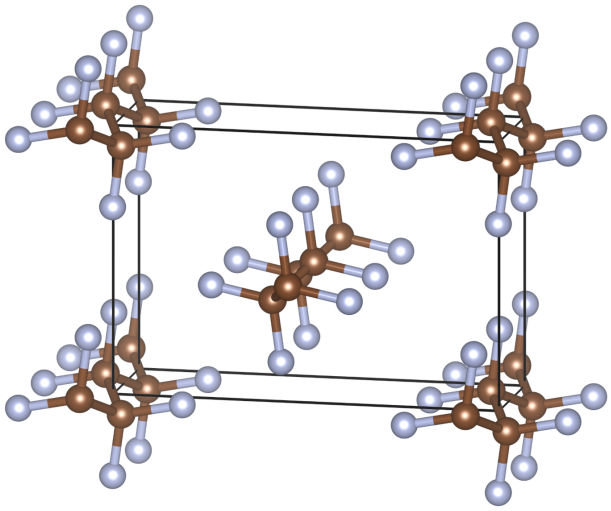

Figure 8: Orthorhombic ($Pnma$) DFT-relaxed crystal structures drawn to scale of (a) polyethylene and (b) polytetrafluoroethylene (PTFE). Both relaxations used the PBE functional and a D3 dispersion correction.[57,58]

mental structure while for the relaxed structure κ_{DFT} is 2.64. These can be compared with the empirical estimate for polyethylene of 2.3.[49] The calculated κ_{DFT} for PTFE was 2.38, close to the reported experimental value of 2.1.[56] As discussed previously, the measured dielectric constants at 10 GHz for paraffin wax (expected to be similar to polyethylene) and PTFE are 2.2 and 2.1, respectively. These observations demonstrate that DFT-calculated values of the dielectric constant for organic molecules are not especially prone to underestimation. Neither do they appear to be sensitive to small changes in structure.

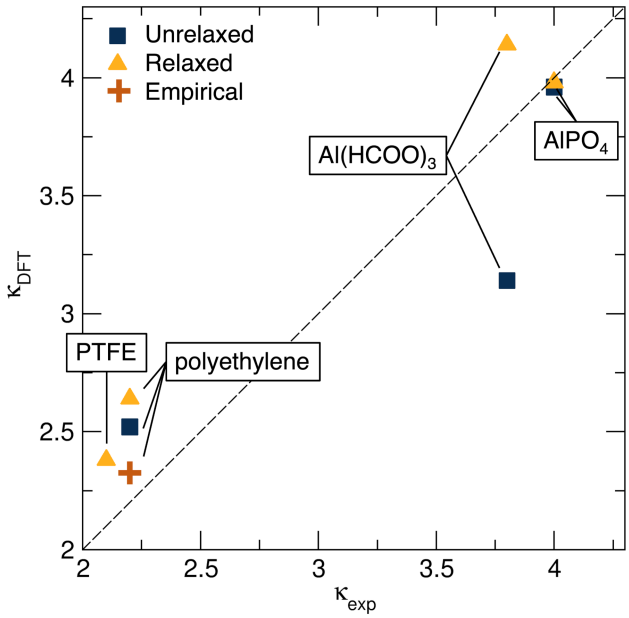

Figure 9: DFT-estimated dielectric constants for un-relaxed and relaxed crystal structures compared with measured values at a frequency of 10.159 GHz. For polyethylene, the experimental value is compared with measurements on cast paraffin wax. The DFT model for PTFE required relaxation, as there is no experimental structure for a commensurate structure in the $Pnma$ space group.

Figure 9 displays the experimentally measured (at a frequency of 10.159 GHz) dielectric constants for PTE, paraffin, $Al(HCOO)_3$, and $AlPO_4$, compared with the empirical value and with DFT calculations on the experimental (unrelaxed) and DFT-relaxed crystal structures. The calculated and empirical values for polyethylene are compared with measurements on chemically similar paraffin. These measurements provide additional validation of the experimental methods employed here since the measured values for paraffin and

PTFE correspond closely to values in the literature.[49,56] Furthermore, the predicted dielectric constants for the polymers and the relaxed structure of $Al(HCOO)_3$ show similar levels variation when compared to experimental data. This suggests that there is something unique about the structure of $Al(HCOO)_3$ determined by neutron diffraction which makes its calculated dielectric constant especially sensitive to structural changes, perhaps associated with finite temperature effects that are beyond the scope of this work.

Conclusion

In this work we have identified the key characteristics of low-κ materials and suggest an effective workflow for searching for these compounds. Additionally, we highlight both the advantages and drawbacks of empirical and DFT estimates of the dielectric constant. Our results demonstrate that empirical methods are useful for sorting through large databases of candidate low-κ materials, while DFT calculations are better-suited for determining which materials to prioritize. Although it remains challenging to identify materials with dielectric constants lower than that of silica ($\kappa < 3.82$ at 10 GHz), we have found that certain aluminum-based materials are close to achieving these low values. We believe that this is due to the high charge on aluminum and its ability to form open, 3D-connected, networks. In the case of $AlPO_4$, the predicted dielectric constant from DFT calculations was nearly identical to the constant determined from measurements. In contrast, for $Al(HCOO)_3$, there was a significant discrepancy between the constant predicted from the experimental crystal structure and experiment. This is because even minor changes in the crystal structure seem to contribute to a significantly higher dielectric constant, which is highlighted by calculating the dielectric constant of a DFT-relaxed structure. The origins of the unique sensitivity of the dielectric constant of $Al(HCOO)_3$ on minute details of the crystal structure could potentially arise from finite-temperature effects that are beyond the scope of the present work.

Supporting Information

FTIR spectra of $Al(HCOO)_3$ before and after heat treatment (Figure S1), dielectric measurements of PTFE composite pellets (Figure S2), loss values for measurements of materials in paraffin wax (Table S1), and Python code to calculate the empirical dielectric constant from an input CIF file.

Acknowledgments

RS thanks Jakoah Brgoch and Ya Zhuo for their help during initial stages of this work, and Susanne Stemmer for helpful discussions. This work was supported by the BASF Corporation through the California Research Alliance CARA). Use of the Shared Experimental Facilities of the National Science Foundation (NSF) Materials Research Science and Engineering Center (MRSEC) at UC Santa Barbara (NSF DMR-2308708) and of the Institute for Terahertz Science and Technology at UC Santa Barbara is gratefully acknowledged. We additionally acknowledge computational support from the Center for Scientific Computing, supported by the NSF CNS-1725797 and NSF DMR-2308708. E.E.M. acknowledges the NSF Graduate Research Fellowship Program under award number 2139319. A.Z. gratefully acknowledges the Elings Postdoctoral Fellowship Program for support. B.M. acknowledges support from a UKRI Future Leaders Fellowship (MR/V023926/1), from the Gianna Angelopoulos Programme for Science, Technology, and Innovation, and from the Winton Programme for the Physics of Sustainability. A.K.C. thanks the Ras Al Khaimah Center for Advanced Materials for financial support.

References

(1) Hill, M. D.; Cruickshank, D. B.; MacFarlane, I. A. Perspective on Ceramic Materials for 5G wireless Communication Systems. *Appl. Phys. Lett.* **2021**, *118*, 120501.

(2) Zhou, Y. Material Foundation for Future 5G Technology. *Acc. Mater. Res.* **2021**, *2*, 306–310.

(3) Shamiryan, D.; Abell, T.; Iacopi, F.; Maex, K. Low-k Dielectric Materials. *Mater. Today* **2004**, *7*, 34–39.

(4) Wang, H. J.; Sun, X. Q.; Bian, J. J. Preparation, Phase Assemblage and Microwave Dielectric Properties of $AlPO_4$-BPO_4-SiO_2 Ternaries. *J. Eur. Ceram. Soc.* **2021**, *41*, 3438–3444.

(5) Morgen, M.; Ryan, E. T.; Zhao, J.-H.; Hu, C.; Cho, T.; Ho, P. S. Low Dielectric Constant Materials for ULSI Interconnects. *Annu. Rev. Mater. Sci.* **2000**, *30*, 645–680.

(6) Kohl, P. A. Low–Dielectric Constant Insulators for Future Integrated Circuits and Packages. *Annu. Rev. Chem. Biomol. Eng.* **2011**, *2*, 379–401.

(7) Volksen, W.; Miller, R. D.; Dubois, G. Low Dielectric Constant Materials. *Chem. Rev.* **2010**, *110*, 56–110.

(8) Lou, W.; Mao, M.; Song, K.; Xu, K.; Liu, B.; Li, W.; Yang, B.; Qi, Z.; Zhao, J.; Sun, S.; Lin, H.; Hu, Y.; Zhou, D.; Wang, D.; Reaney, I. M. Low Permittivity Cordierite-Based Microwave Dielectric Ceramics for 5G/6G Telecommunications. *J. Eur. Ceram. Soc.* **2022**, *42*, 2820–2826.

(9) Ohsato, H.; Kagomiya, I.; Terada, M.; Kakimoto, K. Origin of Improvement of Q Based on High Symmetry Accompanying Si–Al Disordering in Cordierite Millimeter-Wave Ceramics. *J. Eur. Ceram. Soc.* **2010**, *30*, 315–318.

(10) Ohsato, H.; Varghese, J.; Vahera, T.; Kim, J. S.; Sebastian, M. T.; Jantunen, H.; Iwata, M.; Ohsato, H.; Varghese, J.; Vahera, T.; Kim, J. S.; Sebastian, M. T.; Jantunen, H.; Iwata, M. Micro/Millimeter-Wave Dielectric Indialite/Cordierite Glass-Ceramics Applied as LTCC and Direct Casting Substrates: Current Status and Prospects. *J. Korean Ceram. Soc* **2019**, *56*, 526–533.

(11) Kumari, P.; Tripathi, P.; Parkash, O.; Kumar, D. Low Temperature Sintering and Characterization of MgO-B_2O_3-SiO_2 Glass-Ceramics for LTCC Substrate Applications. *Trans. Indian Ceram. Soc.* **2016**, *75*, 229–233.

(12) Došler, U.; Kržmanc, M. M.; Suvorov, D. The Synthesis and Microwave Dielectric Properties of $Mg_3B_2O_6$ and $Mg_2B_2O_5$ Ceramics. *J. Eur. Ceram. Soc.* **2010**, *30*, 413–418.

(13) Hong, W. B.; Li, L.; Yan, H.; Wu, S. Y.; Yang, H. S.; Chen, X. M. Room-Temperature-Densified H_3BO_3 Microwave Dielectric Ceramics With Ultra-Low Permittivity and Ultra-High Qf Value. *J. Materiomics* **2020**, *6*, 233–239.

(14) Ling, H.; Acharya, M.; Martin, L. W.; Persson, K. A. Theory-Guided Exploration of the $Sr_2Nb_2O_7$ System for Increased Dielectric and Piezoelectric Properties and Synthesis of Vanadium-Alloyed $Sr_2Nb_2O_7$. *Chem. Mater.* **2022**, *34*, 8536–8543.

(15) Wu, F.; Zhou, D.; Du, C.; Xu, D.-M.; Li, R.-T.; Shi, Z.-Q.; Darwish, M. A.; Zhou, T.; Jantunen, H. Design and Fabrication of a Satellite Communication Dielectric Resonator Antenna with Novel Low Loss and Temperature-Stabilized $(Sm_{1-x}Ca_x)(Nb_{1-x}Mo_x)O_4$ ($x = 0.15 – 0.7$) Microwave Ceramics. *Chem. Mater.* **2022**, *35*, 104–115.

(16) Ma, J.; Zhang, J.; Guo, J.; Li, X.; Guo, S.; Huan, Y.; Wang, J.; Zhang, S.-T.; Wang, Y. Achieving Ultrahigh Energy Storage Density in Lead-Free Sodium Niobate-Based Ce-

ramics by Modulating the Antiferroelectric Phase. *Chem. Mater.* **2022**, *34*, 7313–7322.

(17) Acharya, M.; Ling, H.; Lou, D.; Ramesh, M.; Hanrahan, B.; Velarde, G.; Asta, M.; Persson, K.; Martin, L. W. Exploring the Morphotropic Phase Boundary in Epitaxial $PbHf_{1-x}Ti_xO_3$ Thin Films. *Chem. Mater.* **2022**, *34*, 9613–9623.

(18) Li, S.; Wang, Y.; Yang, M.; Xu, S.; Liu, M.; Li, Q.; Miao, J.; Guo, E.-J.; Jin, K.; Gu, L.; Zhang, Q.; Deng, J.; Chen, X.; Xing, X. Ferroelectricity in Low-Permittivity $SrZrO_3$ Epitaxial Films. *Chem. Mater.* **2023**, *35*, 2967–2974.

(19) Lee, Y.; Kim, K.; Lee, Z.; Lee, H.-S.; Lee, H.-B.-R.; Kim, W.-H.; Oh, I.-K.; Kim, H. Dysprosium Incorporation for Phase Stabilization of Atomic-Layer-Deposited HfO_2 Thin Films. *Chem. Mater.* **2023**, *35*, 2312–2320.

(20) Bersuker, I. B. Jahn–Teller and Pseudo-Jahn–Teller Effects: From Particular Features to General Tools in Exploring Molecular and Solid State Properties. *Chem. Rev.* **2020**, *121*, 1463–1512.

(21) Laurita, G.; Seshadri, R. Chemistry, Structure, and Function of Lone Pairs in Extended Solids. *Acc. Chem. Res.* **2022**, *55*, 1004–1014.

(22) Woodward, P. M.; Karen, P.; Evans, J. S.; Vogt, T. *Solid State Materials Chemistry*; Cambridge University Press, 2021.

(23) Shannon, R. D. Dielectric Polarizabilities of Ions in Oxides and Fluorides. *J. Appl. Phys.* **1993**, *73*, 348–366.

(24) Evans, H. A.; Mullangi, D.; Deng, Z.; Wang, Y.; Peh, S. B.; Wei, F.; Wang, J.; Brown, C. M.; Zhao, D.; Canepa, P.; Cheetham, A. K. Aluminum Formate, $Al(HCOO)_3$: An Earth-Abundant, Scalable, and Highly Selective Material for CO_2 Capture. *Sci. Adv.* **2022**, *8*, eade1473.

(25) Mullangi, D.; Evans, H. A.; Yildirim, T.; Wang, Y.; Deng, Z.; Zhang, Z.; Mai, T. T.; Wei, F.; Wang, J.; Hight Walker, A. R.; Brown, C. M.; Zhao, D.; Canepa, P.; Cheetham, A. K. Noncryogenic Air Separation Using Aluminum Formate $Al(HCOO)_3$ (ALF). *J. Am. Chem. Soc.* **2023**, *145*, 9850–9856.

(26) Zhang, Z.; Deng, Z.; Evans, H. A.; Mullangi, D.; Kang, C.; Peh, S. B.; Wang, Y.; Brown, C. M.; Wang, J.; Canepa, P.; Cheetham, A. K.; Zhao, D. Exclusive Recognition of CO_2 from Hydrocarbons by Aluminum Formate with Hydrogen-Confined Pore Cavities. *J. Am. Chem. Soc.* **2023**, *145*, 11643–11649.

(27) Jain, P.; Ramachandran, V.; Clark, R. J.; Zhou, H. D.; Toby, B. H.; Dalal, N. S.; Kroto, H. W.; Cheetham, A. K. Multiferroic Behavior Associated with an Order-Disorder Hydrogen Bonding Transition in Metal-Organic Frameworks (MOFs) with the Perovskite ABX_3 Architecture. *J. Am. Chem. Soc.* **2009**, *131*, 13625–13627.

(28) Besara, T.; Jain, P.; Dalal, N. S.; Kuhns, P. L.; Reyes, A. P.; Kroto, H. W.; Cheetham, A. K. Mechanism of the Order–Disorder Phase Transition, and Glassy Behavior in the Metal-Organic Framework $[(CH_3)_2NH_2]Zn(HCOO)_3$]. *Proc. National Acad. Sci. U.S.A.* **2011**, *108*, 6828–6832.

(29) Kresse, G.; Hafner, J. *Ab Initio* Molecular-Dynamics Simulation of the Liquid-Metal–Amorphous-Semiconductor Transition in Germanium. *Phys. Rev. B* **1994**, *49*, 14251–14269.

(30) Kresse, G.; Furthmüller, J. Efficiency of Ab-Initio Total Energy Calculations for Metals and Semiconductors using a Plane-Wave Basis Set. *Comput. Mater. Sci.* **1996**, *6*, 15–50.

(31) Kresse, G.; Furthmüller, J. Efficient Iterative Schemes for *Ab Initio* Total-Energy Calculations Using A Plane-Wave Basis Set. *Phys. Rev. B* **1996**, *54*, 11169–11186.

(32) Perdew, J. P.; Burke, K.; Ernzerhof, M. Generalized Gradient Approximation Made Simple. *Phys. Rev. Lett.* **1996**, *77*, 3865–3868.

(33) Blöchl, P. E. Projector Augmented-Wave Method. *Phys. Rev. B* **1994**, *50*, 17953–17979.

(34) Kresse, G.; Joubert, D. From Ultrasoft Pseudopotentials to the Projector Augmented-Wave Method. *Phys. Rev. B* **1999**, *59*, 1758–1775.

(35) Monkhorst, H. J.; Pack, J. D. Special Points for Brillouin-zone Integrations. *Phys. Rev. B* **1976**, *13*, 5188–5192.

(36) Baroni, S.; Resta, R. Ab initio Calculation of the Macroscopic Dielectric Constant in Silicon. *Phys. Rev. B* **1986**, *33*, 7017–7021.

(37) Gajdoš, M.; Hummer, K.; Kresse, G.; Furthmüller, J.; Bechstedt, F. Linear Optical Properties in the Projector-Augmented Wave Methodology. *Phys. Rev. B* **2006**, *73*, 045112.

(38) Petousis, I.; Chen, W.; Hautier, G.; Graf, T.; Schladt, T. D.; Persson, K. A.; Prinz, F. B. Benchmarking Density Functional Perturbation Theory to Enable High-Throughput Screening of Materials for Dielectric Constant and Refractive Index. *Phys. Rev. B* **2016**, *93*, 115151.

(39) Hashin, Z.; Shtrikman, S. Conductivity of Polycrystals. *Phys. Rev.* **1963**, *130*, 129–133.

(40) Tian, Y.-Q.; Zhao, Y.-M.; Xu, H.-J.; Chi, C.-Y. CO_2 Template Synthesis of Metal Formates with a ReO_3 Net. *Inorg. Chem.* **2007**, *46*, 1612–1616.

(41) Coelho, A. A. TOPAS and TOPAS-Academic: An Optimization Program Integrating Computer Algebra and Crystallographic Objects Written in C++. *J. Appl. Crystallogr.* **2018**, *51*, 210–218.

(42) Momma, K.; Izumi, F. VESTA 3 for Three-Dimensional Visualization of Crystal, Volumetric and Morphology Data. *J. Appl. Crystallogr.* **2011**, *44*, 1272–1276.

(43) Tempke, R.; Wildfire, C.; Shekhawat, D.; Musho, T. Dielectric Measurement of Powdery Materials Using a Coaxial Transmission Line. *IET Sci., Meas. Technol.* **2020**, *14*, 972–978.

(44) Krupka, J.; Clarke, R.; Rochard, O.; Gregory, A. Split Post Dielectric Resonator Technique for Precise Measurements of Laminar Dielectric Specimens-Measurement Uncertainties. 13th International Conference on Microwaves, Radar and Wireless Communications. 2000; pp 305–308.

(45) Krupka, J.; Geyer, R. G.; Baker-Jarvis, J.; Ceremuga, J. Measurements of the Complex Permittivity of Microwave Circuit Board Substrates using Split Dielectric Resonator and Reentrant Cavity Techniques. 1996.

(46) Looyenga, H. Dielectric Constants of Heterogeneous Mixtures. *Physica* **1965**, *31*, 401–406.

(47) Xie, C.; Oganov, A. R.; Dong, D.; Liu, N.; Li, D.; Debela, T. T. Rational Design of Inorganic Dielectric Materials with Expected Permittivity. *Sci. Rep.* **2015**, *5*, 16769.

(48) Takahashi, A.; Kumagai, Y.; Miyamoto, J.; Mochizuki, Y.; Oba, F. Machine Learning Models for Predicting the Dielectric Constants of Oxides Based on High-Throughput First-Principles Calculations. *Phys. Rev. Mater.* **2020**, *4*, 103801.

(49) Newnham, R. E. *Properties of Materials: Anisotropy, Symmetry, Structure*; Oxford University Press, 2005.

(50) Hellenbrandt, M. The Inorganic Crystal Structure Database (ICSD) – Present and Future. *Crystallogr. Rev.* **2004**, *10*, 17–22.

(51) Bhagavantham, S.; Narayana Rao, D. A. A. S. Dielectric Constant of Diamond. *Nature* **1948**, *161*, 729.

(52) Lew, C. M.; Cai, R.; Yan, Y. Zeolite Thin Films: From Computer Chips to Space Stations. *Acc. Chem. Res.* **2009**, *43*, 210–219.

(53) Jain, A.; Ong, S. P.; Hautier, G.; Chen, W.; Richards, W. D.; Dacek, S.; Cholia, S.; Gunter, D.; Skinner, D.; Ceder, G.; Persson, K. A. Commentary: The Materials Project: A Materials Genome Approach to Accelerating Materials Innovation. *APL Mater.* **2013**, *1*, 011002.

(54) Groom, C. R.; Bruno, I. J.; Lightfoot, M. P.; Ward, S. C. The Cambridge Structural Database. *Acta Crystallogr. B* **2016**, *72*, 171–179.

(55) Shi, G.; Zhang, F.; Zhang, B.; Hou, D.; Chen, X.; Yang, Z.; Pan, S. $Na_2B_6O_9F_2$: A Fluoroborate with Short Cutoff Edge and Deep-Ultraviolet Birefringent Property Prepared by an Open High-Temperature Solution Method. *Inorg. Chem.* **2016**, *56*, 344–350.

(56) Wall, L. A. *Fluoropolymers*; Wiley-Interscience: New York,, 1972.

(57) Grimme, S.; Antony, J.; Ehrlich, S.; Krieg, H. A Consistent and Accurate Ab Initio Parametrization of Density Functional Dispersion Correction (DFT-D) for the 94 elements H-Pu. *J. Chem. Phys.* **2010**, *132*, 154104.

(58) Grimme, S.; Ehrlich, S.; Goerigk, L. Effect of the Damping Function in Dispersion Corrected Density Functional Theory. *J. Comput. Chem.* **2011**, *32*, 1456–1465.

(59) Miao, M. S.; Zhang, M.-L.; Van Doren, V. E.; Van Alsenoy, C.; Martins, J. L. Density Functional Calculations on the Structure of Crystalline Polyethylene Under High Pressures. *J. Chem. Phys.* **2001**, *115*, 11317–11324.

(60) Fatti, G.; Righi, M. C.; Dini, D.; Ciniero, A. First-Principles Insights into the Structural

and Electronic Properties of Polytetrafluoroethylene in Its High-Pressure Phase (Form III). *J. Phys. Chem. C* **2019**, *123*, 6250–6255.

(61) Bunn, C. W.; Howells, E. R. Structures of Molecules and Crystals of Fluoro-Carbons. *Nature* **1954**, *174*, 549–551.

TOC Graphic

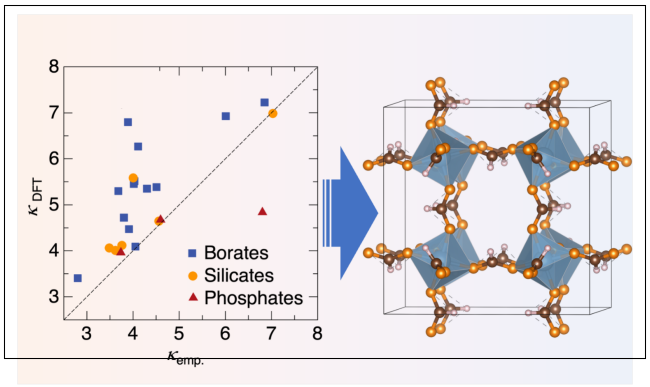
8
7
6
5
4
3
3
4
5
6
7
8
κ_{DFT}
$\kappa_{emp.}$
Borates
Silicates
Phosphates

SUPPORTING INFORMATION FOR

Screening Aluminum-Based Compounds as Low-κ Dielectrics for High-Frequency Applications

Emily E. Morgan,[†,‡] Arava Zohar,[†,‡] Sophia Lipkin,[¶] Bartomeu Monserrat,[§] Subramanian Vaidyanathan,[‖] Daniel Loeffler,[‖] Rui Zhang,[⊥] Kerstin Schierle-Arndt,[‖] Anthony K. Cheetham,[‡,#] and Ram Seshadri[*,‡,¶]

[†]*These authors contributed equally to this work*

[‡]*Materials Department and Materials Research Laboratory University of California, Santa Barbara, California 93106, United States*

[¶]*Department of Chemistry and Biochemistry*
University of California, Santa Barbara, California 93106, United States

[§]*Department of Materials Science and Metallurgy and Cavendish Laboratory University of Cambridge, Cambridge CB3 0FS, United Kingdom*

[‖]*BASF SE, 67056 Ludwigshafen am Rhein, Germany*

[⊥]*California Research Alliance (CARA)*
BASF Corporation, Berkeley, California 94720, United States

[#]*Department of Materials Science and Engineering*
National University of Singapore, Singapore 117575, Singapore

E-mail: seshadri@mrl.ucsb.edu

Table of contents

Section S1. FTIR of $Al(HCOO)_3$

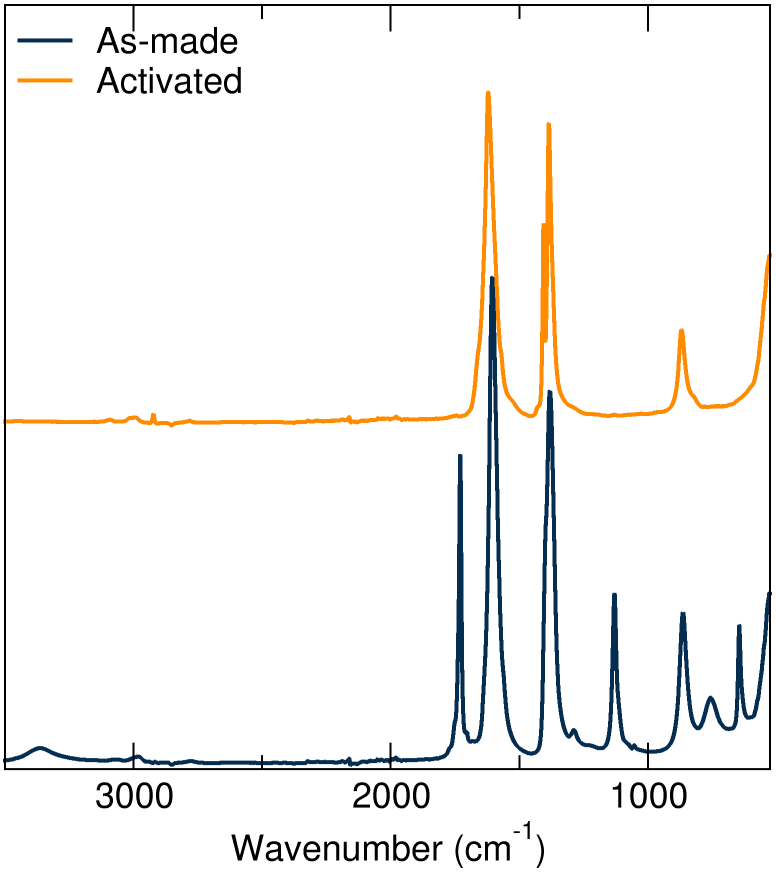

Figure S1. FTIR spectra of $Al(HCOO)_3$ before and after heat treatment at 180 °C.

Section S2. Dielectric measurements of PTFE pellets

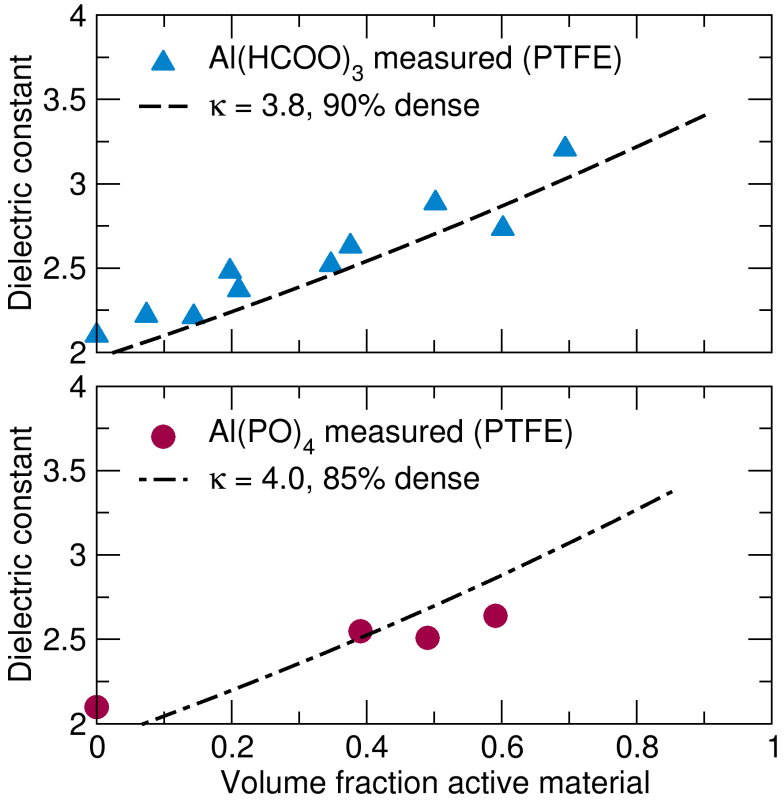

Figure S2. Dielectric measurements of $Al(HCOO)_3$ and $AlPO_4$ mixtures with PTFE and associated curves generated from the Looyenga mixing model.

Section S3. Dielectric loss values associated with the measurements of materials in waxes.

SiO_2	
Volume fraction	Average loss
0	4.12×10^{-4}
0.185	5.59×10^{-4}
0.254	6.53×10^{-4}
0.338	7.18×10^{-4}
0.443	7.03×10^{-4}
0.577	7.84×10^{-4}
$Al(HCOO)_3$	
Volume fraction	Average loss
0.209	3.48×10^{-3}
0.292	7.29×10^{-3}
0.382	1.00×10^{-2}
$AlPO_4$	
Volume fraction	Average loss
0.144	1.11×10^{-3}
0.208	1.18×10^{-3}
0.371	1.67×10^{-3}

Table S1. Average dielectric loss values associated with the measurements of materials in waxes.

Section S4. Example Python code which can be used to estimate the dielectric constant from a given CIF obtained from the ICSD

```
import pandas as pd

import numpy as np

import re

import math

polarizabilities = {"Li" : 1.20, "Be" : 0.19, "B" : 0.05, "O" : 2.01, "F" : 1.62, "Na" : 1.80, "Mg" : 1.32, "Al" : 0.79, "Si" : 0.87, "P" : 1.22, "K" : 3.83, "Co" : 1.65, "Ni" : 1.23, "Cu" : 2.11, "Zn" : 2.04, "Ga" : 1.50, "Ge" : 1.63, "As" : 1.72}

lines = []

with open('cif_name_here','rt') as cif:

        for line in cif:

                lines.append(line.rstrip('\n'))

formulaline = [match for match in lines if "_chemical_formula_sum" in match]

volumeline = [match for match in lines if "_cell_volume" in match]

unitsline = [match for match in lines if "_cell_formula_units_Z" in match]

cellvolume = re.findall('\d*\.?\d+', volumeline[0])

cellvolume = float(cellvolume[0])

formulaunits = re.findall('\d*\.?\d+', unitsline[0])

formulaunits = int(formulaunits[0])

formulavolume = cellvolume/formulaunits

elements = re.findall('[A-Z][a-z]?',formulaline[0])

elementnum = re.findall('\d*\.?\d+',formulaline[0])

elementinfo = [elements,elementnum]

calcalpha = pd.DataFrame(elementinfo).transpose()

calcalpha.columns = ['element', 'number']

calcalpha = calcalpha.replace({'element': polarizabilities})

calcalpha = calcalpha.astype(float)

calcalpha['alphas'] = calcalpha['element'] * calcalpha['number']

totalalpha = calcalpha['alphas'].sum()
```

```
constant = (formulavolume+2*totalalpha*(4*math.pi/3))/(formulavolume-
totalalpha*(4*math.pi/3))

print(constant)
```